Nuclear Engineering and Technology 53 (2021) 3367–3378

Contents lists available at ScienceDirect

Nuclear Engineering and Technology

journal homepage: www.elsevier.com/locate/net

Original Article

Assessment of three European fuel performance codes against the SUPERFACT-1 fast reactor irradiation experiment

L. Luzzi [a, *], T. Barani [a], B. Boer [b], L. Cognini [a], A. Del Nevo [c], M. Lainet [d], S. Lemehov [b], A. Magni [a], V. Marelle [d], B. Michel [d], D. Pizzocri [a], A. Schubert [e], P. Van Uffelen [e], M. Bertolus [d]

[a] Politecnico di Milano, Department of Energy, Nuclear Engineering Division, via La Masa 34, 20156, Milano, Italy
[b] Studiecentrum voor Kernenergie (SCK·CEN), Boeretang 200, 2400 Mol, Belgium
[c] ENEA, FSN-ING-SIS, CR Brasimone, 40032, Camugnano (BO), Italy
[d] Commissariat à l'Energie Atomique et aux Energies Alternatives, CEA DEC/SESC, 13108, St. Paul Lez Durance, France
[e] European Commission, Joint Research Centre, Directorate for Nuclear Safety and Security, P.O. Box 2340, 76125, Karlsruhe, Germany

ARTICLE INFO

Article history:
Received 11 December 2020
Received in revised form
8 April 2021
Accepted 9 April 2021
Available online 15 April 2021

Keywords:
SUPERFACT-1 irradiation experiment
Fuel performance
GERMINAL
MACROS
TRANSURANUS
MOX fuel
Assessment and benchmark

ABSTRACT

The design phase and safety assessment of Generation IV liquid metal-cooled fast reactors calls for the improvement of fuel pin performance codes, in particular the enhancement of their predictive capabilities towards uranium-plutonium mixed oxide fuels and stainless-steel cladding under irradiation in fast reactor environments. To this end, the current capabilities of fuel performance codes must be critically assessed against experimental data from available irradiation experiments. This work is devoted to the assessment of three European fuel performance codes, namely GERMINAL, MACROS and TRANSURANUS, against the irradiation of two fuel pins selected from the SUPERFACT-1 experimental campaign. The pins are characterized by a low enrichment (~ 2 wt.%) of minor actinides (neptunium and americium) in the fuel, and by plutonium content and cladding material in line with design choices envisaged for liquid metal-cooled Generation IV reactor fuels. The predictions of the codes are compared to several experimental measurements, allowing the identification of the current code capabilities in predicting fuel restructuring, cladding deformation, redistribution of actinides and volatile fission products. The integral assessment against experimental data is complemented by a code-to-code benchmark focused on the evolution of quantities of engineering interest over time. The benchmark analysis points out the differences in the code predictions of fuel central temperature, fuel-cladding gap width, cladding outer radius, pin internal pressure and fission gas release and suggests potential modelling development paths towards an improved description of the fuel pin behaviour in fast reactor irradiation conditions.

1. Introduction

The future of innovative Generation IV reactors [1,2] foresees the development of various liquid-metal cooled fast reactors[1] (i.e., ASTRID and ESFR, sodium-cooled [3,4]; ALFRED, lead-cooled [5]; MYRRHA, cooled by lead-bismuth eutectic [6]). The current design of all these innovative demonstrators and commercial-size reactors features (U, Pu) mixed oxide fuel (MOX), with cladding materials belonging to the family of 15–15Ti austenitic stainless steels. Fuel performance codes (FPCs) need development and validation efforts to assess the fuel pin design for fast reactor irradiation conditions and to verify the compliance with pin safety requirements (e.g., margin to fuel melting, cladding plastic strain, as applied for the fuel pin design of ALFRED [7]).

Among the phenomena governing the fuel pin performance under irradiation, the behaviour of MOX fuel is crucial and needs to be targeted by dedicated modelling efforts. The improvement of the current modelling of MOX properties in FPCs, integrating experimental and lower-length scale researches is the ultimate objective of the INSPYRE H2020 European Project (Investigations Supporting

* Corresponding author.
E-mail address: lelio.luzzi@polimi.it (L. Luzzi).

[1] Other Generation IV reactor concepts under development are e.g., the Very-High Temperature Reactor (VHTR), mainly helium-cooled and employing TRISO particle fuel; the Gas-cooled Fast Reactor (GFR), still helium-cooled, of which ALLEGRO is the most representative concept; the Molten Salt Fast Reactor (MSFR) and the Supercritical Water-cooled Reactor (SCWR) [1].

https://doi.org/10.1016/j.net.2021.04.010

MOX Fuel Licensing for ESNII Prototype Reactors) [8]. The three FPCs under assessment in INSPYRE are GERMINAL, developed by CEA, France [9,10]; MACROS, from SCK●CEN, Belgium [11]; and TRANSURANUS, developed by JRC-Karlsruhe, Germany [12,13].[2] While GERMINAL is specifically tailored to fast reactor (sodium-cooled) irradiations, TRANSURANUS is a code system primarily applied to light water reactor (LWR) conditions and extended to take into account fast neutron spectra and further specific material properties for fast reactor applications [12,13]. MACROS is a mechanistic code that can be applied both to LWR fuels and to fast reactor (FR) systems.

Among the irradiation campaigns whose information and experimental results are available to the European FPC community, the SUPERFACT-1 irradiation experiment [14] has been selected as part of the INSPYRE FPC assessment strategy as representative of MOX fuel irradiation in sodium fast reactor environment. Moreover, the minor actinide content (americium and neptunium) in the SUPERFACT-1 pellets allows the analysis of the behaviour of nuclear fuel under fast neutron irradiation for transmutation purposes. This is recognized as an important path to follow in the development of future Generation IV liquid metal-cooled fast reactors, allowing for the ultimate radioactive waste management and sustainability improvement by better use of nuclear fuel resources [15]. As a first step, the versions of the GERMINAL, MACROS and TRANSURANUS codes at the beginning of the INSPYRE Project were employed to simulate two pins from the SUPERFACT-1 irradiation experiment, with the aim of assessing the simulation capabilities of the codes prior to the improvements developed during the INSPYRE Project.

The simulation outcomes concerning the selected fuel pins from the SUPERFACT-1 irradiation experiment are herein presented and critically discussed. First, the results from each involved code are compared to the available experimental measurements, consisting in both integral and local post-irradiation examination data [14,16,17]. Then, the employed FPCs are benchmarked by comparing the evolution during irradiation of quantities of engineering interest.

The paper is organized as follows. Section 2 reports the description and main specifications of the SUPERFACT-1 irradiation experiment, while Section 3 provides a brief description of the three codes used for the simulation of the SUPERFACT-1 pins considered. Sections 4 and 5 collect the result of the pin performance simulations in terms of assessment against available experimental data and code-to-code benchmark, respectively. Potential paths of further development arising from this work are mentioned in Section 6 and conclusions are drawn in Section 7.

2. The SUPERFACT-1 irradiation experiment

The SUPERFACT-1 irradiation experiment was jointly conducted by CEA, France and ITU, now JRC-Karlsruhe, Germany, between 1984 and 1993 in the Phénix sodium-cooled fast reactor [14]. The goal of the experiment was to investigate how mixed oxide fuel, doped with small contents of the minor actinides (MAs) Np and Am, behaves under irradiation in a fast spectrum reactor, to demonstrate the feasibility of MA transmutation through homogeneous (i.e., low MA content) and heterogeneous (i.e., high MA content) fuel concepts [16]. In this work, the focus is on the homogeneous concepts, represented by the fuel pins SF7 and SF13, bearing 2 wt.% of ^{237}Np, and by the pins SF4 and SF16, bearing 1.8 wt.% of ^{241}Am. The irradiation of the fuel manufactured at ITU took place in the Phénix reactor between the 38th and 42nd cycles (October 1986 – January 1988). The maximum linear power reached during the experiment was around 38.7 kW/m, while the peak fuel burnup at the end of life was about 6.5 at.% and the peak cladding damage about 52 NRT-dpa.[3] Post irradiation examinations (PIEs) were performed both at CEA and ITU, covering a wide set of non-destructive and destructive analyses [14,16,17].

The as-fabricated geometry and the characteristics of the considered pins are reported in Table 1 [18]. The fuel pin consists of a stack of solid pellets, all with the same composition, and a cladding made of 15–15Ti stabilized, cold-worked austenitic stainless steel. The geometric dimensions of the fuel-to-cladding gap, upper and lower plenum are reported in Table 1. A spring is present in the upper plenum to hold the fuel stack in position during the loading procedures. The sodium coolant conditions and channel properties are reported in Table 2 [18].

The evolution in time of the linear heat rate and fast neutron flux (i.e., neutrons with energy above 200 keV) in the cladding is reported in Fig. 1, scaled with respect to the respective maximum

Table 1
Design parameters of the considered fuel pins from the SUPERFACT-1 irradiation experiment [14].

Parameter	SF7 and SF13	SF4 and SF16
Pellet radius (mm)	2.68	2.71
Radial gap (mm)	0.143	0.116
Pellet density (%TD)[a]	97.5	96.3
Initial fuel grain diameter (μm)	10	10
U[b]/M (wt./)	0.741	0.745
MA/M (wt./)	0.02,^{237}Np	0.018,^{241}Am
Pu[c]/M (wt./)	0.244	0.237
O/M	1.943	1.957
Fuel column mass (g)	207.24	209.61
Fissile column length (mm)	850	
Cladding material	15-15, Ti stabilized, cold-worked stainless steel	
Cladding thickness (mm)	0.45	
Upper plenum volume (mm^3)	1930	
Lower plenum volume (mm^3)	19530	
Helium (filling gas) pressure (MPa)	0.1	
Helium (filling gas) temperature (°C)	20	

[a] Theoretical Densities: 11.077 g/cm^3 for the Np-bearing MOX (pins SF7 and SF13), 11.131 g/cm^3 for the Am-bearing MOX (pins SF4 and SF16).
[b] Natural uranium composition.
[c] ^{238}Pu 1.3 wt.%,^{239}Pu 60.4 wt.%,^{240}Pu 23.4 wt.%,^{241}Pu 10.4 wt.%,^{242}Pu 4.5 wt.%.

Table 2
Details about the sodium coolant properties and the coolant channel geometry of the SUPERFACT-1 irradiation experiment [14]. The data reported refer to the single fuel pins considered in this work.

Parameter	Value
Na mass flow rate (kg/s)	0.098
Na inlet temperature (°C)	395
Na pressure (MPa)	0.1
Coolant area (mm^2)	22.55
Hydraulic diameter (mm)[a]	4.997

[a] The hydraulic diameter is calculated through the (reported) coolant channel area and the wetted perimeter. This information disregards the pin array disposition and refers to an equivalent pipe flow.

[2] CEA performed the work herein presented with GERMINAL V2.2.5, SCK●CEN with the MACROS code, while ENEA, JRC-Karlsruhe and Politecnico di Milano employed version v1m1j20 of the TRANSURANUS code.

[3] The Norgett–Robinson–Torrens displacements per atom (NRT-dpa) model is the current international standard for quantifying the energetic particle damage of the lattice of a material [86].

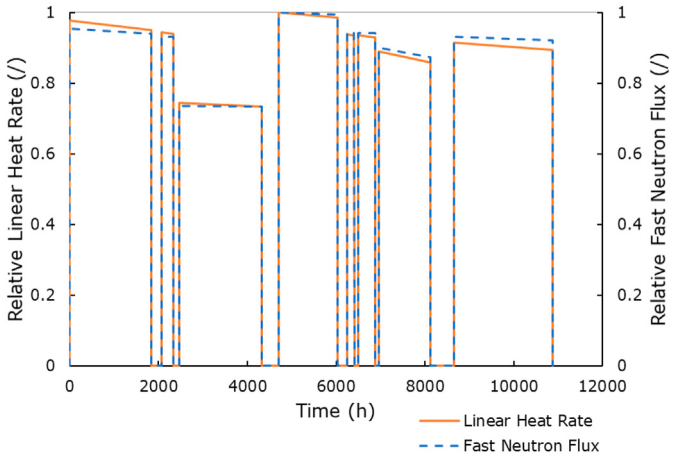

Fig. 1. Relative linear heat rate and fast neutron flux (above 200 keV), with respect to their maximum values, as a function of time for the considered fuel pins (both Am- and Np-bearing pins) [14].

values. After the shutdown, the fuel pins were stored for 1020 days before PIE analyses were performed. The axial power and flux shapes are defined through peak factors (Table 3), as a result of which the peak power node (ppn) is located slightly below the half of the active fuel column, i.e., at 382.5 mm from the bottom of fuel column (bfc). Complete information about the SUPERFACT-1 irradiation history is collected in [18], based on [14].

The assessment activity herein performed is deliberately focused on the best-estimate code results, to gain knowledge about the current level of accuracy of the involved fuel performance codes.

3. Code comparative description

This section provides a brief comparative description of the three fuel performance codes involved in this work. It is intended as a support to the interpretation of the simulation results presented and analysed in the following Sections 4 and 5. The code structure, main numerical features and recommended modelling choices, suitable for the materials and irradiation conditions of the SUPERFACT-1 experiment, are mentioned and referenced.

TRANSURANUS [12,13,19] is a computer code for the thermal and mechanical analysis of fuel rods irradiated in nuclear reactors (both thermal and fast, i.e., light water or liquid-metal cooled, respectively), designed to simulate both normal, transient and accidental conditions. TRANSURANUS is referred to as a "1.5-D" code, meaning that the thermal and mechanical analysis is performed radially in both fuel and cladding, and then the solved radial profiles are coupled between different axial slices of the fuel column. The code is equipped with both physical models and empirical engineering-level correlations, aiming at bridging the fuel grain scale (and related phenomena, e.g., the fission gas behaviour) with the integral scale of the fuel pin. The TRANSURANUS modelling choices for properties and phenomena of fuel, cladding and coolant, employed for the simulation of the SUPERFACT-1 irradiation experiment, correspond to the code recommended models to describe the behaviour under irradiation of fast reactor MOX fuels, 15-15Ti cladding steel and liquid sodium coolant [12,13] (e.g, correlation for MOX fuel thermal conductivity according to Philipponneau [20], employed also by GERMINAL). As for the code modelling of the main processes occurring in the fuel and cladding under irradiation, TRANSURANUS is currently equipped with suitable models for:

- Intra- and inter-granular fission gas behaviour [21,22], accounting for grain boundary saturation [23], grain growth and grain boundary sweeping effects [24].
- A FR-tailored model for fuel-cladding gap conductance, accounting for enhanced fuel-cladding contact, based on [25].
- Redistribution of actinides (Pu, Am) in FR conditions [26] and of oxygen via thermo-diffusion [27].
- Porosity migration leading to fuel densification [28,29] and restructuring (formation of fuel central void and columnar grains) [30].
- Fuel cracking, both macro- (at the pellet level) and micro- (at the grain boundary level), in the fragile pellet regions, depending on temperature and burnup and determining the release of the corresponding gas inventory [12].
- Swelling and creep (both thermal and irradiation-induced) of fuel [28,31,32] and cladding [7,33].
- High Burnup Structure formation at the fuel pellet periphery (above a threshold burnup and for sufficiently low temperatures) [34].

The GERMINAL code is developed on a generic numerical approach of the PLEIADES fuel software environment developed by the CEA [10]. The multi-physics algorithm is based on a coupling formulation with three main behaviours: thermal, mechanical, and physico-chemical. The computation scheme is based on a two-scale model with a local multi-physics coupling formulation in each axial slice of the fuel pin and a global description for integral state variables such as internal pressure, fission gas release, coolant power evacuation. The current version of GERMINAL includes a fuel pin model with a 1D approach for each slice of the axial discretization. The local thermomechanical computation is based on the multi-dimensional Cast3M finite element solver embedded in the PLEIADES software environment. The thermal model can describe the heat transfer through the pellet, the gap and the cladding under steady state and transient conditions up to the melting of the pellet.

Table 3
Axial nodalization applied to the SUPERFACT-1 fuel pins considered in this work, together with the peak factors (defined as local-to-peak ratios) defining the axial profile of the pin linear power and fast neutron flux [14,18].

Axial slice number	Height of the slice centre from bottom of fuel column (mm)	Axial peak factors (/)
1	42.5	0.572
2	127.5	0.737
3	212.5	0.868
4	297.5	0.958
5	382.5	1
6	467.5	0.983
7	552.5	0.912
8	637.5	0.802
9	722.5	0.658
10	807.5	0.498

The mechanical model describes the quasi-static equilibrium of the pellet and the cladding according to a non-linear behaviour and unilateral contact condition at the pellet-cladding interface. Constitutive equations used for the non-linear mechanical behaviour are based on the Hooke law and an additive formulation of the inelastic strains. The latter include creep, plasticity, fuel relocation and volume changes due to thermal expansion and irradiation. For physico-chemical aspects a set of models are used to describe:

- Central hole formation and fuel restructuring through a vaporization-condensation process.
- Fuel densification and swelling under irradiation.
- Spatial redistribution of actinides and oxygen.
- Radial evolution of the chemical composition in the pellet.
- Fission gas behaviour (release and swelling).
- Fuel and cladding chemical behaviour, including the formation and evolution of the JOG (Joint Oxyde-Gaine) layer in the fuel-cladding gap. The JOG is a layer consisting of fission product compounds [35], filling the fuel-cladding gap of high burnup, fast reactor fuel pins and observed from post-irradiation examinations [36]. It is determined by the release from the fuel pellets of volatile fission products and associated compounds generated in the fuel, enhanced by the high-temperature regime of FR pins, and its formation starts at a sufficiently high fuel burnup (~ 70 GWd/t, from the currently available experimental observations [35,37,38]).

Detailed features of the GERMINAL computation scheme are available in an extended paper [9], with the constitutive equations solved by the code given in [10]. The material parameters are derived from the GERMINAL validation with the SFR (Sodium Fast Reactor) experimental data base and updated based on the recommendations from the ESNII + Project [39].

The MACROS code was originally developed for the modelling and analysis of in-reactor behaviour of non-standard mixed oxide fuels (e.g., inert matrices and targets with elevated concentrations of minor actinides [40–43]). The MACROS code consists of several modules:

- Neutronic module to model fuel depletion and/or build-up of actinides and the main fission products (e.g., Cs, Mo, I) [44].
- Module to simulate material properties of homogeneous mixed oxides (based on thoria, urania-plutonia or zirconia) and heterogeneous targets (based on MgO, Mo, and SiC) [40,45,46].
- Module to simulate the in-pile properties of materials that are currently used or considered as claddings for LWR, LMFBR (Liquid-Metal Fast Breeder Reactor) and ADS (Accelerator-Driven System) pins [45,47].
- Module to simulate diffusional fission gas release, in-pile densification, porosity evolution and gas swelling, including formation and size distributions of intra-granular nanometric bubbles, inter-granular pores on grain faces, edges and corners [11]. This module also relies on the results of molecular dynamics simulations for some specific parameters involved in the diffusional process (e.g., activation energies and volumes of defects associated with vacancies, interstitials and inert gases – Xe, Kr and He) [48–52].
- Module to simulate fuel-side and coolant-side corrosion and cladding oxidation [53].
- Module to simulate fuel cracking and fragmentation in steady-state conditions and accidental transients (LOCAs and RIAs, i.e., Loss Of Coolant Accidents and Reactivity-Initiated Accidents, respectively) [54,55].
- Standard models to calculate pin pressure, gap conductance, and other thermal-mechanical integral properties.

4. Comparison against experimental data

The overall comparison with the integral data shown in Table 4 for the Am-bearing pin is deemed satisfactory, although few specific issues arise. TRANSURANUS overpredicts the axial extent of the fuel central hole in both considered fuel pins, which can be ascribed to an overall overprediction of the temperature regime along the fuel column. Moreover, predictions of fuel column elongation do not compare well with the experimental data, being strongly overpredicted by TRANSURANUS and MACROS while underpredicted by GERMINAL. A correct estimation and assessment of fuel elongation remains difficult, considering the complexity of the mechanisms involved in the elongation process, which is also influenced by fuel axial relocation and by the constrained boundary conditions induced by the pellet-cladding gap closure. Another difficulty for the assessment activity is linked to the uncertainty on the fuel column elongation measurements, as the free parts of the fuel stack may move when the fuel pin is handled during post-irradiation examinations. On the contrary, the agreement with the experimental volume of fission gases produced during irradiation is remarkable, while the measured integral fission gas release is generally underestimated by the three codes. Finally, the volumes of helium release estimated by TRANSURANUS and MACROS are in reasonable and good agreement with experimental values, respectively. The GERMINAL prediction is overestimated because of the assumption of total release of the generated helium.

The comparison of the calculated cladding outer diameter at the end of life (including the storage time before PIEs) with the experimental cladding profilometries is reported in Fig. 2, for the SF13 (Np-doped) and SF16 (Am-doped) fuel pins. The overall agreement of the simulation results with the experimental measurements is satisfactory. In particular, the agreement of the GERMINAL predictions with data from the Np-pin is excellent, thanks to its refined cladding swelling model based on the large experimental database available at the CEA [9]. The cladding diametrical deformations at the end of life calculated by TRANSURANUS and MACROS are slightly different for the Am- and Np-pins, whereas no differences are observed in the GERMINAL results. These different predictions between codes, which remain within the experimental uncertainties [14], can be mainly explained by the initial pin outer diameters employed by the GERMINAL computations, which are similar and higher compared to the values reported in Table 1 (6.555 and 6.554 mm instead of 6.552 and 6.546 mm, for the Am- and Np-pins, respectively). These differences can also be ascribed to the different empirical correlations employed to calculate the cladding swelling rate, to the temperature and dose thresholds triggering the swelling and to the different correlations employed to compute cladding creep. Both irradiation-induced and thermal creep are considered by the codes: TRANSURANUS solves the constitutive equations for the non-linear mechanical behaviour, including the creep and swelling treatment in an additive formulation of inelastic strains [12,33]. GERMINAL solves these equations as well, but uses different creep and swelling correlations [9]. The different treatments of fuel creep and swelling can partially justify the discrepancies in the cladding profilometry predictions, especially where fuel-cladding gap closure takes place, predicted by GERMINAL and MACROS as shown in Fig. 11 of Section 4 for the peak power node. Then, as displayed by Fig. 2, the maximum cladding diameter measured experimentally is located below the peak power node, where the temperature is deemed not

Table 4
Comparison of experimental data [14] and simulation results of integral quantities regarding the americium-bearing fuel pins (SF4, SF16).

	Measured	Calculated TRANSURANUS	Calculated GERMINAL	Calculated MACROS
Final burnup at ppn (at.%)	6.4	6.35	6.60	6.60
Fission gas (Xe + Kr) produced (cm^3)	225.03	226.40	226.68	236.40
Fission gas release (%)	68.5	47.00	53.15	53.80
Kr/(Kr + Xe) (%)	6.85	6.88	7.14	6.94
Helium released (cm^3)	39.7[a]	28.15	60.88[b]	38.00
Central hole length (mm)	550–619	691.00	424.69	541.00
Fuel elongation (mm)	5.6–6.2	25.50	0.47	39.13
Cladding elongation (mm)	1.5–2.3	1.43	−0.01	1.76

[a] Measurement after 20 months from shutdown.
[b] Result obtained with a 100% release assumption.

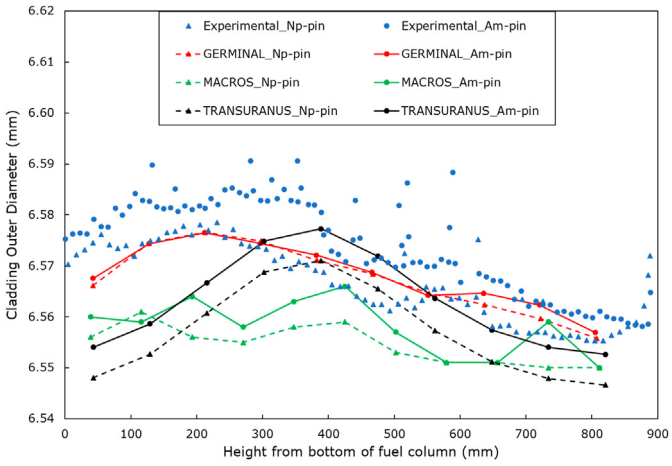

Fig. 2. Assessment of the calculated cladding axial profilometry at the end of life, for the Np-bearing pin SF13 (triangles, dashed lines) and the Am-bearing pin SF16 (circles, full lines), against experimental measurements.

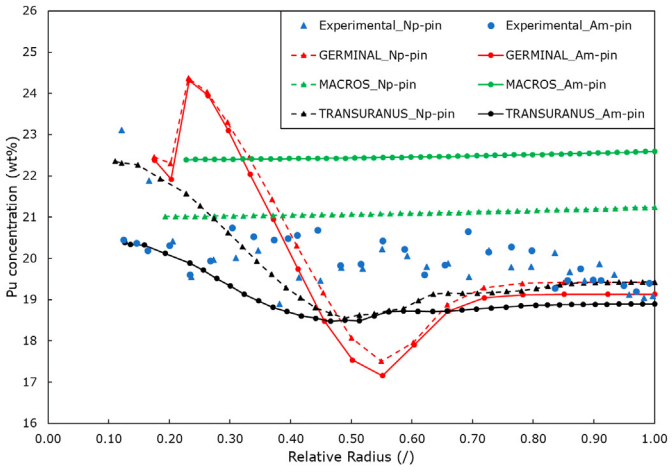

Fig. 3. Assessment of the calculated plutonium radial concentration at the end of life, at the axial peak power node, for the Np-bearing pin SF13 (triangles, dashed lines) and the Am-bearing pin SF16 (circles, full lines), against experimental measurements.

high enough to activate a recovery process able to reduce the swelling rate, despite a higher dose at the peak power node. This effect is well represented by GERMINAL, while TRANSURANUS predictions are largely determined by the axial shape of the linear power (and fast neutron flux, Table 3), suggesting a predominant impact of irradiation swelling and creep on the predicted cladding profilometry at the end of life. The different dependencies on the irradiation damage of the correlations employed by the codes for cladding swelling and creep prove to be the main cause of discrepancies in the code calculations shown in Fig. 2, together with the contribution of fuel-cladding mechanical interaction in case of the gap closure predicted by GERMINAL and MACROS (Fig. 11). MACROS results show a general underestimation of the experimental profilometries.

The calculated radial profiles of plutonium concentration at the peak power node are compared with corresponding experimental data in Fig. 3, showing a remarkable agreement of TRANSURANUS predictions with the measurements. Also GERMINAL provides a satisfactory agreement at the pellet periphery. These codes predict a substantial redistribution of plutonium across the pellet, which is consistent with PIE outcomes. This effect is, however, overestimated by GERMINAL, i.e., a stronger migration of plutonium from the intermediate pellet radii to the inner pellet region is observed. The MACROS code is not equipped with a redistribution model so far. The models employed by GERMINAL and TRANSURANUS (considered as the best-estimate ones for fast reactor MOX fuel in their state-of-the-art code version) rely on several parameters and include dependencies on local quantities impacting on the performance results (e.g., the oxygen-to-metal ratio (O/M), above all) [9,56]. The modelling and values of these parameters are still preliminary, subject to large uncertainties and open to revisions and improvements. In the range of O/M ratios corresponding to slightly hypo-stoichiometric fuel (O/M between 1.97 and 2.00), the partial vapour pressures of U and Pu oxides are similar, so there is not a preferential redistribution of one element compared to the other [29,57,58]. The lack of sensitivity to the O/M ratio represents a current limitation of the redistribution process modelling and calls for a comprehensive thermo-chemical modelling of the fuel under irradiation [9,59], in combination with dedicated experiments and atomic scale simulations (e.g., [60]).

The predictions of neptunium (SF13 pin) and americium (SF16 pin) radial concentrations at the peak power node are compared to experimental data in Fig. 4. Under fast reactor conditions, americium is subject to redistribution due either to solid-state diffusion or evaporation-condensation mechanisms because of the steep radial temperature gradient and high temperature levels. On the contrary, neptunium is considered to be less or even not affected by redistribution mechanisms [26,61,62]. The TRANSURANUS model for actinide redistribution therefore considers only plutonium and americium redistribution [26], whereas the evolution of the neptunium radial concentration during irradiation is only determined by fuel burnup. The GERMINAL code also includes a model for neptunium redistribution [9], while the flat MACROS results are consistent with the fact that its burnup module is not yet coupled to an actinide redistribution model [11]. The code predictions agree satisfactorily with the experimental results for both neptunium and americium, considering the experimental uncertainties [16,17]. The accuracy of GERMINAL calculations is remarkable, although

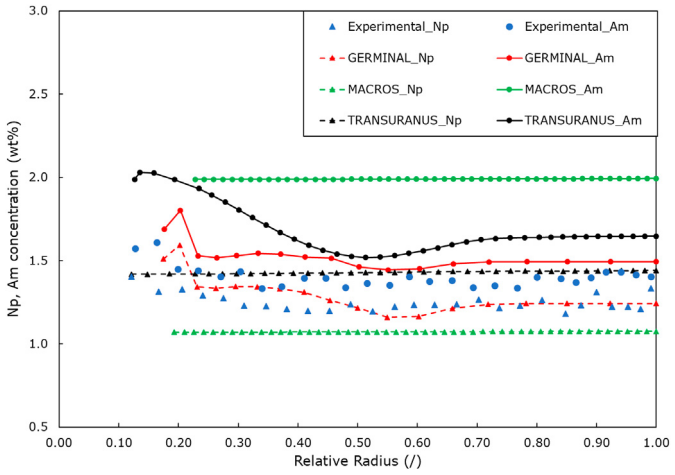

Fig. 4. Assessment of the calculated neptunium radial concentration (for the Np-bearing pin SF13 - triangles, dashed lines) and of the calculated americium radial concentration (for the Am-bearing pin SF16 - circles, full lines), at the end of life, at the axial peak power node, against experimental measurements.

showing a concentration step close to the central void, due to a numerical artefact which allows moving from the finite volume mesh (used to solve the porosity migration equation) to the finite element mesh of the multi-physics formulation. TRANSURANUS overestimates the radial redistribution of americium and the average concentrations of Am and Np at the end of life, which could point to a required revision of some cross-sections of the code database.

Comparisons of measured against predicted xenon and caesium radial concentrations in the two pins considered are presented in Fig. 5 and Fig. 6, respectively. As for xenon, the concentration is well caught by MACROS and TRANSURANUS in the inner and outer regions of the pellet, while some discrepancies arise at the intermediate radii. This result indicates that the onset of fission gas release for the SUPERFACT-1 fuels simulated here is not evaluated properly by the two codes. Regarding GERMINAL calculations, the increase of Xe concentration at the pellet periphery is linked to a threshold temperature below which gas release does not occur (i.e., the intragranular diffusion coefficient features a thermal activation term) [9]. Only MACROS yields the same Xe concentration radial profiles

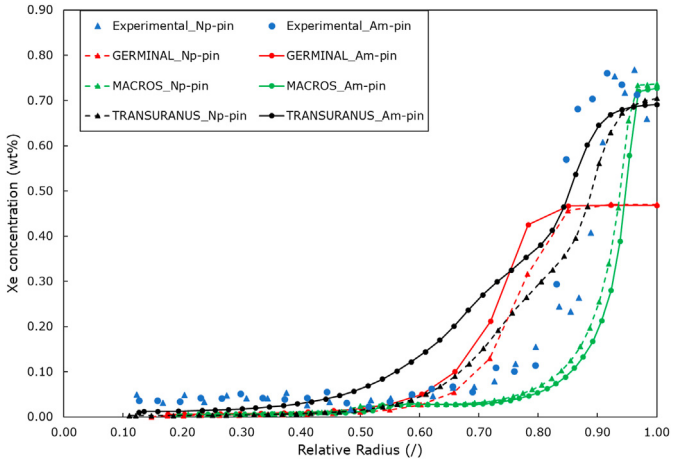

Fig. 5. Assessment of the calculated xenon radial concentration at the end of life, at the axial peak power node, for the Np-bearing pin SF13 (triangles, dashed lines) and the Am-bearing pin SF16 (circles, full lines), against experimental measurements.

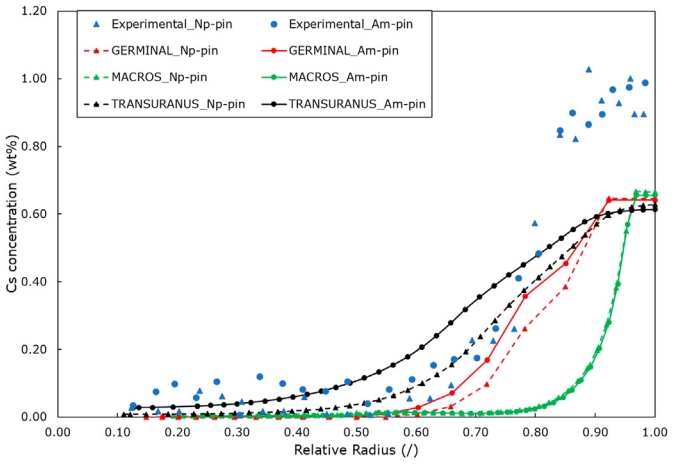

Fig. 6. Assessment of the calculated caesium radial concentration at the end of life, at the axial peak power node, for the Np-bearing pin SF13 (triangles, dashed lines) and the Am-bearing pin SF16 (circles, full lines), against experimental measurements.

between the Am-pin and the Np-pin, both underestimating the experimental data at the inner and intermediate radii. As for caesium, the code predictions are based on a simplified description of its production, evolution and release by fuel grains. For example, in TRANSURANUS and GERMINAL the caesium release is correlated to the xenon one [9,12], in models which do not account for the various possible compounds caesium can form and their possible phases (solid, liquid, vapour or gaseous, depending on local temperature and oxygen potential). Hence, the current models cannot reproduce the higher experimental concentrations measured in the outermost region of the pellet, which can be ascribed to axial caesium migration neglected in the employed state-of-the-art codes. Also, the MACROS code predicts an increase in the concentration of Cs retained in the fuel grains starting at higher radii, implying a significant underestimation of the measured caesium profiles in the intermediate pellet region, which is the most challenging region for code simulations. It is worth pointing out that the retained concentrations of fission gas and fission products in the outer region of the fuel pellets and their release in the fuel-cladding gap are in principle also influenced by the formation and evolution of the High Burnup Structure (HBS), a fuel microstructure evolution towards smaller grains and elevated porosity occurring at sufficiently high burnup and low temp eratures < 1000°C [34,63,64]. The HBS formation and its effects on the fission gas behaviour dynamics (e.g., depletion of fission gases from the fuel matrix and accumulation in the HBS pores) are implemented in the TRANSURANUS code, as mentioned in Section 3, but not considered for the fuels simulated in this work. A partial fuel recrystallization in the SUPERFACT-1 SF13/16 pins has been observed [17], but the final peak burnup reached during the experiment (~ 65 GWd/t) suggests a limited formation of the HBS. Indeed, the HBS is experimentally observed to start at local fuel burnups between 60 and 75 GWd/t, but its dynamics are still under investigations [65,66].

The assessment of the code predictions against PIE experimental data on the axial profiles of fuel inner diameter and columnar grain diameter at the end of life is presented in Fig. 7 and Fig. 8, respectively. Focusing first on the inner void diameter predictions (Fig. 7), TRANSURANUS predictions of the inner void diameter are remarkable, but reveal clearly different profiles compared to GERMINAL and MACROS axial results. The central void formation in TRANSURANUS and GERMINAL is computed from a multi-physics formulation coupling thermo-mechanical aspects and fuel

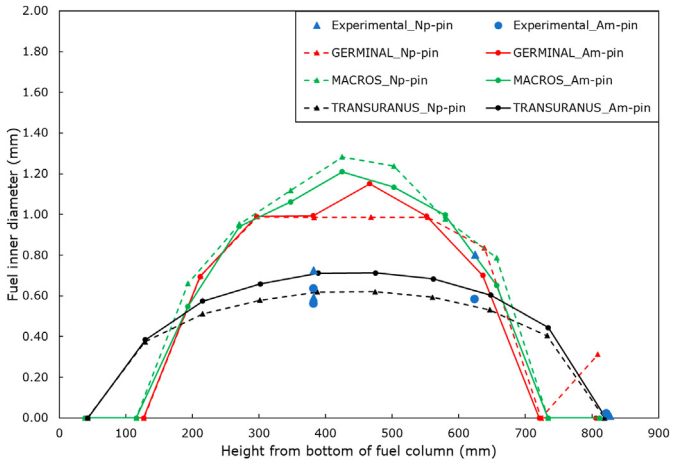

Fig. 7. Assessment of the calculated axial profiles of fuel inner diameter at the end of life, for the Np-bearing pin SF13 (triangles, dashed lines) and the Am-bearing pin SF16 (circles, full lines), against experimental measurements. Where two measurements of the same quantity are available at the same position, they refer to different measurements carried out at CEA and ITU, yielding different values.

restructuring through a vaporization-condensation process and porosity migration, and involving specific model parameter fitting [9,12]. The restructuring model in MACROS (accounting for the coupled formation of columnar grains and central void) adopts a semi-empirical approach linking the local radial temperatures with the characteristic restructuring propagation time. The MACROS model features an activation energy associated with the vaporization/sublimation processes and a minimal temperature required as onset of fuel restructuring (set to 1800°C), consistently with experimental observations [11,67]. As mentioned above in the discussion of the integral results, TRANSURANUS overpredicts the axial extent of the inner void (but correctly predicts the observed absence of a central void at the top of the fuel column at the end of life), which should be linked to an overprediction of the fuel central temperature. The latter is also indicated by the predictions of the columnar grain region diameter, reported in Fig. 8. Indeed, the agreement of GERMINAL and MACROS results on the extension of columnar grains with the experimental data is good (despite the overestimation of the inner void size at the end of life), while TRANSURANUS tends to overpredict the extension of this region, implying an overestimation of the fuel temperature regime. There is no fuel restructuring at the active fuel column extremities according to both GERMINAL and MACROS simulation results. GERMINAL predicts an unusual opening of the fuel central void at the top of the fuel column in the Np-bearing pin, linked to a local overestimation of the fuel temperature due to an overestimation of the gap size. This suggest the need for improvements concerning the modelling of the coupled effects between central hole formation, fuel restructuring and pellet-cladding gap closure, involving also a better formulation of the relocation model (see e.g., [68]). It is worth noting that the inner void diameter final value may be affected not only by fuel restructuring, which usually takes place at the beginning of irradiation, but possibly also by fuel inward creep, which can occur if fuel-cladding contact is established.

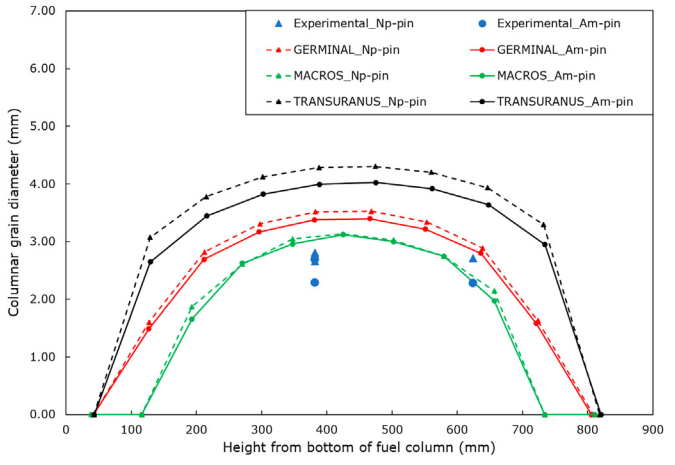

Fig. 8. Assessment of the calculated axial profiles of columnar grain diameter at the end of life, for the Np-bearing pin SF13 (triangles, dashed lines) and the Am-bearing pin SF16 (circles, full lines), against experimental measurements. Where two measurements of the same quantity are available at the same position, they refer to different measurements carried out at CEA and ITU, yielding different values.

5. Benchmark of fuel performance codes

In this Section, the evolution during irradiation of quantities of engineering interest, which were not measured during the experimental campaign, is presented and discussed to provide a deeper analysis and understanding of the different models included in the fuel performance codes herein applied.

In Fig. 9, the predictions of the fuel central temperature evolution at the peak power node of the fuel pins considered are compared. Significant discrepancies can be noticed in the temperature regimes predicted by the codes, in terms of both values and dynamics, especially in the early reactor cycles while smoothing out towards the end of irradiation. In particular, the biggest differences concern the SUPERFACT-1 Np-pin, reaching up to five hundred degrees during the second reactor cycle. Generally, TRANSURANUS provides the highest temperature regimes, while GERMINAL yields the lowest ones. These discrepancies may be ascribed to different approaches adopted in the codes to model the fuel radial relocation (stochastic in nature and subject to large uncertainties): the TRANSURANUS model is based on [31,69], while it is computed in GERMINAL through an empirical formulation with fitted parameters. Also, different modelling of gap conductance accounting for gap closure, of fuel creep and thermal expansion impact on the predicted fuel temperatures [9,12,69]. Additionally, the fuel central temperature decrease predicted by GERMINAL during the first and the second power cycles is linked to the increase of the fuel oxygen-to-metal ratio (O/M) due to the

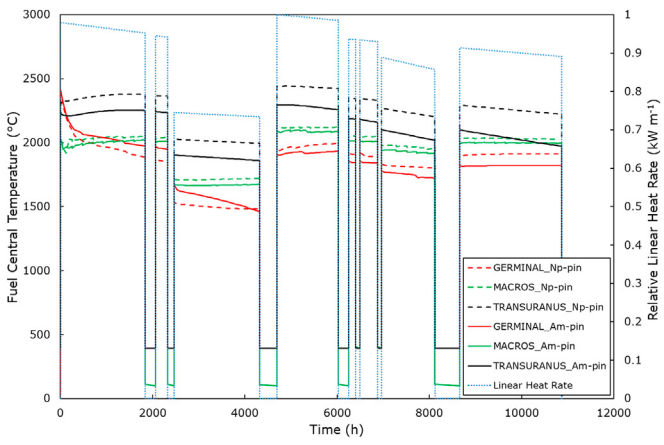

Fig. 9. Evolution of the calculated fuel central temperature along irradiation, at the peak power node, for the Np-bearing pin SF13 (dashed lines) and the Am-bearing pin SF16 (full lines).

consumption of fissile atoms. The reduced deviation from stoichiometry (corresponding to O/M = 2.00) results in an improved thermal conductivity of the fuel material, leading consequently to a temperature decrease in the pellets.

The evolution of the fuel inner radius at the peak power node is shown in Fig. 10. Similar dynamics (i.e., fast inner void formation as fuel pins are brought to power) can be recognized in TRANSURANUS and MACROS results, although the asymptotic values predicted by the codes are significantly different (MACROS predicts the formation of the largest central void, coherently with Fig. 7). The fast formation of the largest fuel central void, according to the MACROS modelling, contributes to explain the lower fuel central temperature predicted by MACROS at the beginning of life (Fig. 9). The inner void size evolution predicted by GERMINAL shows a gradual increase along irradiation and is discontinuous due to the discrete finite element mesh used for the computation [9]. However, it follows the power cycles correctly. A similar stepwise central void behaviour is predicted by MACROS, although much less affected by the various power cycles, as in TRANSURANUS calculations after the first rise to power. In general, a slightly higher inner void size in time is predicted for the Am-pin, with the differences among the code results ascribable to the different densification and restructuring models available in the codes [9,11,28,31,70,71].

Fig. 11 showcases the predicted evolution of the fuel-cladding gap size at the peak power node. Again, significant differences arise in the code results, mainly linked to the discrepancies in the predicted temperature regimes (Fig. 9). In particular, MACROS and GERMINAL predict a fast closure of the gap in both considered pins at the beginning of irradiation, ascribed to fuel relocation and fuel creep modelling [9,11], while TRANSURANUS predictions suggest a slower closure of the fuel-cladding gap leading to the highest temperature regime predicted in the fuel pellets. The gap never closes according to TRANSURANUS simulations, although it almost reaches closure at the end of irradiation. Also, the effect of gap re-opening when power drops is more pronounced in TRANSURANUS. It is important to underline that, in addition to beginning-of-life phenomena (fuel and cladding sudden thermal expansion, fuel relocation and restructuring), other irradiation phenomena contribute to determine the gap dynamics, such as fuel swelling, cladding creep and swelling. In particular, the differential swelling of fuel and cladding along irradiation is lower from TRANSURANUS calculations compared to GERMINAL and MACROS predictions.

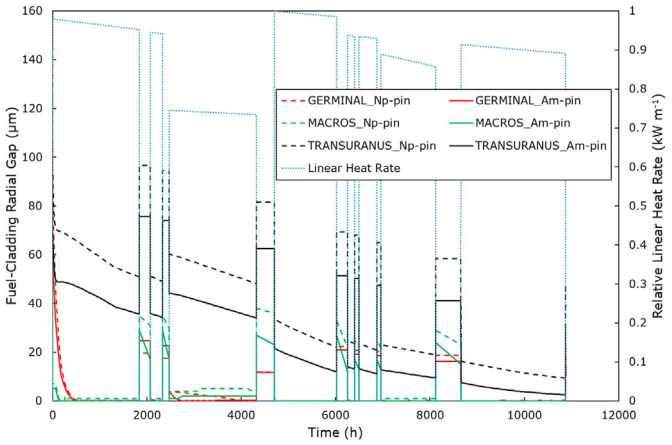

Fig. 11. Evolution of the calculated fuel-cladding radial gap size along irradiation, at the peak power node, for the Np-bearing pin SF13 (dashed lines) and the Am-bearing pin SF16 (full lines).

The evolution of the cladding outer radius at the peak power node is reported in Fig. 12. The values reached at the beginning of life (just after the first raise to power) by the three codes are slightly different, indicating a difference in the linear thermal expansion coefficients considered by the codes [9,11,12,72]. The cladding outer temperature at beginning of life is the lowest from TRANSURANUS calculations (around 500°C). It is slightly higher according to GERMINAL and more than 10°C higher according to MACROS, consistently with a higher cladding thermal expansion after the first power ramp. Moreover, while TRANSURANUS and GERMINAL predict similar trends consistent with the power evolution for both SUPERFACT-1 pins, MACROS results show a stronger effect of power variations and different cladding dynamics between the two pins, in particular during the inter-cycles and towards the end of irradiation. The cladding geometry is affected by fuel-cladding contact (hence, by fuel swelling), cladding creep and swelling. The latter two phenomena are particularly delicate to model and depend significantly on the empirical correlations included in the codes. In particular, TRANSURANUS relies on a correlation predicting the onset of cladding swelling [12], while in GERMINAL the swelling model activates when a threshold incubation dose for swelling to occur is reached at the considered axial position [9].

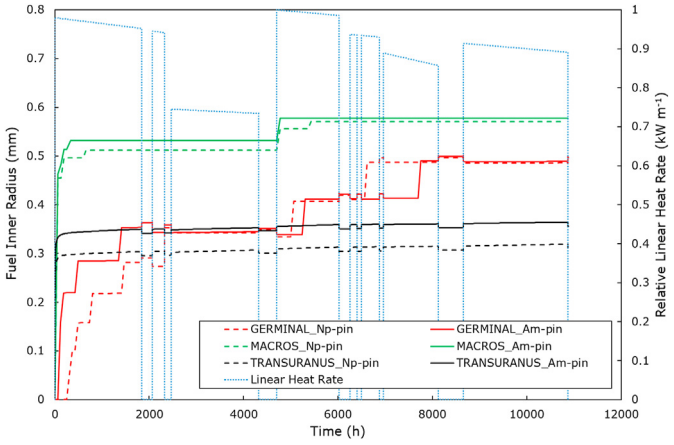

Fig. 10. Evolution of the calculated fuel inner radius along irradiation, at the peak power node, for the Np-bearing pin SF13 (dashed lines) and the Am-bearing pin SF16 (full lines).

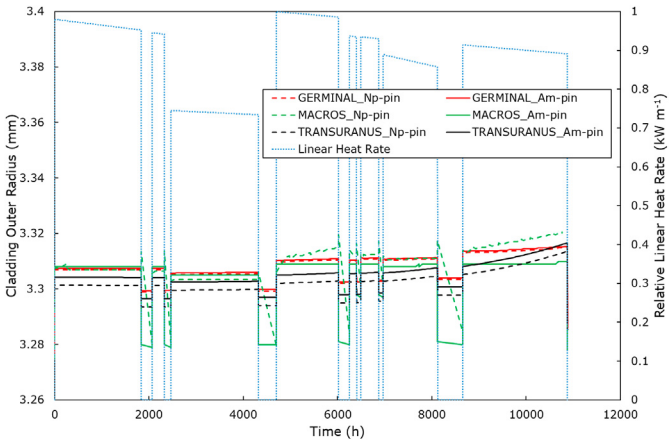

Fig. 12. Evolution of the calculated cladding outer radius along irradiation, at the peak power node, for the Np-bearing pin SF13 (dashed lines) and the Am-bearing pin SF16 (full lines).

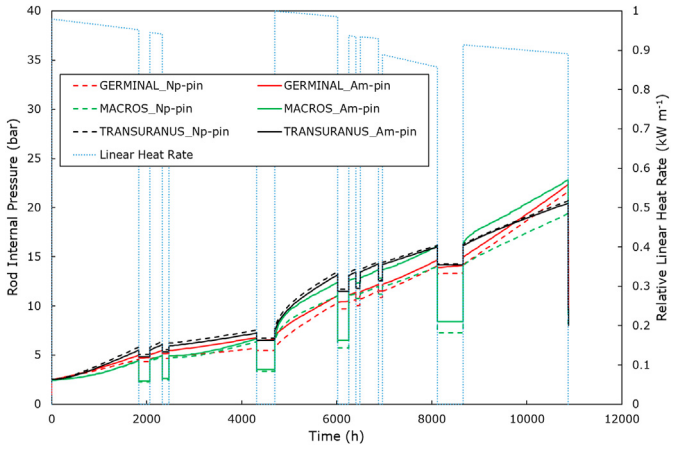

Fig. 13. Evolution of the calculated pin pressure (in the fuel-cladding gap) along irradiation, at the peak power node, for the Np-bearing pin SF13 (dashed lines) and the Am-bearing pin SF16 (full lines).

The predicted evolution of the pin internal pressure and fission gas release, at the peak power node of both pins, are reported in Fig. 13 and Fig. 14, respectively. Both quantities are largely determined by the temperature regime experienced by the fuel column during irradiation, hence the differences in the predicted temperature regimes (Fig. 9) reflect on these calculations. A significantly different dynamics of fission gas release (Fig. 14) is predicted by TRANSURANUS with respect to GERMINAL and MACROS, i.e., characterized by a fast increase up to ~ 60% during the first reactor cycle (Np-bearing pin), then following the power cycles up to an end-of-irradiation value of ~ 65%. The fission gas release trends predicted by GERMINAL and MACROS also show a pronounced impact of the fourth power cycle, corresponding to the maximum linear power of the entire irradiation history. Fission gas release in TRANSURANUS is computed with a simplified model featuring a threshold for the grain face fractional coverage above which intergranular gas release occurs [73]. In GERMINAL instead, fission gas release is computed with an empirical formulation where the temperature effect is introduced through a thermal activation term [9]. The decrease of the GERMINAL prediction during the third cycle of irradiation, noticeable also in the TRANSURANUS results, is hence caused by the lower operating power during this cycle. The

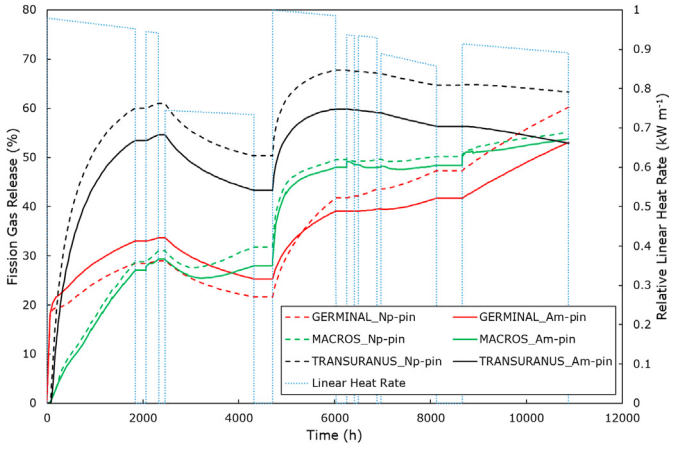

Fig. 14. Evolution of the calculated fission gas release along irradiation, at the peak power node, for the Np-bearing pin SF13 (dashed lines) and the Am-bearing pin SF16 (full lines).

pressures in the fuel-cladding gap (Fig. 13) yielded by all codes for both SUPERFACT-1 pins follow closely and are consistent with the fission gas release evolutions, both in values and in trends.

6. Future developments

The assessment activity presented here shows how the considered fuel performance code predictions exhibit an encouraging agreement with the available experimental data from the SUPERFACT-1 irradiation experiment. Substantial room for improvements, however, clearly emerges from this work. Code development paths related to the INSPYRE Project goals (i.e., the improvement of MOX fuel modelling in fuel performance codes, based on lower-length scale information and applicable to Generation IV reactor conditions) can be identified.

First, the modelling of mixed oxide fuel thermal conductivity in fast reactor conditions demands improvements and further assessment, as suggested mainly by Figs. 7–9. Progress concerning this fuel property would help to improve the prediction of the restructured zone development under irradiation, by enhancing and harmonizing the fuel temperature evolutions calculated by the different codes. Modelling efforts on fast reactor MOX thermal conductivity in the framework of INSPYRE led to the development and validation of an original and comprehensive model, published in [74]. Moreover, improving the fuel relocation modelling (a process of stochastic nature but largely impacting especially in beginning-of-life conditions) would help to reduce the significant spread in the centreline temperature predictions arising from the code calculations (Fig. 9). Progress in describing fuel relocation would also impact the predicted fuel-cladding gap size (Fig. 11), hence an analysis of the relocation impact on the gap conductance involving the investigation of the different models implemented in the codes would be the natural follow-up.

Consequently, temperature-driven phenomena (e.g., fuel thermal creep and densification, influencing the gap dynamics, and fission gas behaviour) would benefit from more accurate predictions of the fuel temperature regime during irradiation. The substantial deviations observed between code predictions of the fuel-cladding gap evolution under irradiation confirm the need for a more accurate fuel mechanical description, which is under investigation in INSPYRE through dedicated experiments and model developments [75,76]. Concerning fission gas behaviour, the comparison of the radial distribution of xenon in the fuel (Fig. 5) and of the integral quantities of fission gases and helium released (Table 4) shows that improvement is also needed on this side, both in the modelling and in the experiments. A mechanistic model of fission gas and helium behaviour in nuclear fuels, including a dedicated treatment of gas release in fast reactor conditions, has recently been developed [34,77,78] and implemented in the SCIANTIX grain-scale code [79], which is currently coupled with the TRANSURANUS and GERMINAL fuel performance codes. The SCIANTIX modelling also enables the description of inert gas behaviour in the high porosity of the High Burnup Structure, developing in the pellet rim (outer) zone above a burnup threshold (between 60 and 75 GWd/t) and at sufficiently low temperatures (below 1000°C, from the currently available experimental observations [65,66]). Although SCIANTIX already includes a refined threshold for matrix depletion and transfer of fission gases in the HBS pores, the mechanism of gas release from the HBS, involving a possible saturation of the pores, is still not assessed in the current literature and is the subject of investigations. This would eventually impact the calculated radial profiles of retained fission gases and the fission gas release in the fuel-cladding gap, with consequences on the overall pin thermal-mechanical performance. The assessment of the SCIANTIX current capabilities for various types of fuel materials

(UO_2, MOX fuels) and irradiation conditions (light water, liquid metal reactor environments) is ongoing. The experimental support is fundamental, since novel and accurate measurements would be highly beneficial to the modelling activity and its validation.

The comparison between experimental and calculation results points out a substantial deviation concerning the radial distributions of volatile fission products (e.g., the radial caesium concentration, Fig. 6), likely due to an unsatisfactory description of their behaviour in mixed oxide fuels. New accurate measurements of fission products concentration in and release from mixed oxide fuels would also bring significant progress in the understanding of the formation and evolution of the fission product (mainly caesium) compounds [80,81], constituting the experimentally observed fuel outer oxide layer referred to as JOG (Joint Oxyde-Gaine) [36]. In close relationship to this, the modelling of the oxygen potential and oxygen-to-metal ratio radial evolution in fuel performance codes, which strongly impacts the volatile fission product behaviour, is also necessary. The current assessed versions of the GERMINAL, MACROS and TRANSURANUS codes only consider the effect of the oxygen radial concentration in the fuel on the thermal properties (e.g., thermal conductivity, melting temperature), although TRANSURANUS also considers the coupling between the oxygen and actinide redistribution [26,27]. Developments ongoing for the GERMINAL code concern the coupling of the multi-physics computational scheme with the OpenCalphad code for thermodynamic computations [38], while the TRANSURANUS code is being coupled with the MFPR-F code for similar purposes [82].

Finally, other identified improvement needs are related to the behaviour of the stainless-steel cladding under irradiation in sodium fast reactor conditions. In particular, the substantial deviations among the code predictions of cladding profilometries (Fig. 2) are likely due to the different correlations and models of cladding creep and void swelling implemented in the codes. The properties of cladding materials for application to Generation IV concepts are under investigation in the ongoing GEMMA H2020 Project [83,84].

7. Conclusions

This work focuses on the assessment of the European fuel performance codes GERMINAL, MACROS and TRANSURANUS against two integral irradiation experiments from the SUPERFACT-1 experimental campaign. The considered pins, made of Am- and Np-bearing mixed-oxide fuel, are representative of pins to be adopted in Generation IV sodium fast reactors in terms of fuel composition, cladding material and irradiation history (i.e., linear power and neutron flux levels). The study presented here is the first step in the assessment strategy of fuel performance codes against fast reactor experimental campaigns carried out in the framework of the INSPYRE H2020 European Project. The pre-INSPYRE versions of the codes were employed to assess and establish their simulation capabilities as a reference for the assessment of the modelling improvements that will be developed in the Project.

The assessment performed shows an encouraging agreement between the predictions of fuel performance codes and available experimental data. It also highlights quantitative differences among the three codes. Several development paths and priorities related to the modelling of MOX fuels in fast reactor conditions are identified as a result of this assessment. The results obtained suggest that, above all, modelling efforts seem to be necessary to improve and harmonize the temperature profile predictions of the three codes. This will impact the numerous temperature-driven phenomena, e.g., fuel thermal creep, influencing the gap dynamics, and fission gas and helium behaviour and release in mixed oxide fuel. In addition, novel accurate measurements would be highly beneficial to the fuel performance code improvement. This is also true for the fuel relocation and fuel-cladding gap conductance models, and especially for beginning-of-life conditions, as pointed out by the different gap evolutions calculated by the codes. The gap size is also affected by the irradiation behaviour of the stainless-steel cladding in liquid metal fast reactor conditions, which is yet to underpin, as suggested by the deviations among the predictions of cladding profilometries. Finally, the integral validation and benchmark herein performed pave the way to additional uncertainty and sensitivity analyses, based on the identification of the topics of primary importance emerging from this work.

The outcomes of this work underline the importance of international collaborations for a more effective improvement and validation of fuel performance codes in the perspective of a reliable analysis of Generation IV reactor concepts. A good example is the new Coordinated Research Project of the IAEA on fuel materials for fast reactors [85], in the frame of which a code benchmark will also be organised.

Declaration of competing interest

The authors declare that they have no known competing financial interests or personal relationships that could have appeared to influence the work reported in this paper.

Acknowledgments

This work has received funding from the Euratom research and training programme 2014–2018 through the INSPYRE Project under grant agreement No 754329.

References

[1] GIF (Generation IV International Forum), GIF R&D Outlook for Generation IV Nuclear Energy Systems - 2018 Update, 2018.
[2] GIF (Generation IV International Forum), Annual Report 2019, 2019.
[3] T. Beck, V. Blanc, J.M. Escleine, D. Haubensack, M. Pelletier, M. Phelip, B. Perrin, C. Venard, Conceptual design of ASTRID fuel sub-assemblies, Nucl. Eng. Des. 315 (2017) 51–60.
[4] ESFR-SMART, ESFR-SMART European H2020 Project [Online]. Available, http://esfr-smart.eu/, 2017.
[5] G. Grasso, C. Petrovich, D. Mattioli, C. Artioli, P. Sciora, D. Gugiu, G. Bandini, E. Bubelis, K. Mikityuk, The core design of ALFRED, a demonstrator for the European lead-cooled reactors, Nucl. Eng. Des. 278 (2014) 287–301.
[6] H.A. Abderrahim, D. De Bruyn, M. Dierckx, R. Fernandez, L. Popescu, M. Schyns, A. Stankovskiy, G. Van Den Eynde, D. Vandeplassche, MYRRHA accelerator driven system programme: recent progress and perspectives, Nucl. Power Eng. 2 (2019) 29–41.
[7] L. Luzzi, A. Cammi, V. Di Marcello, S. Lorenzi, D. Pizzocri, P. Van Uffelen, Application of the TRANSURANUS code for the fuel pin design process of the ALFRED reactor, Nucl. Eng. Des. 277 (2014) 173–187.
[8] EERA-JPNM, INSPYRE - Investigations Supporting MOX Fuel Licensing in ESNII Prototype Reactors [Online]. Available, http://www.eera-jpnm.eu/inspyre/, 2017.
[9] M. Lainet, B. Michel, J.C. Dumas, M. Pelletier, I. Ramière, GERMINAL, a fuel performance code of the PLEIADES platform to simulate the in-pile behaviour of mixed oxide fuel pins for sodium-cooled fast reactors, J. Nucl. Mater. 516 (2019) 30–53.
[10] B. Michel, I. Ramière, I. Viallard, C. Introini, M. Lainet, N. Chauvin, V. Marelle, A. Boulore, T. Helfer, R. Masson, J. Sercombe, J.C. Dumas, L. Noirot, S. Bernaud, Two fuel performance codes of the PLEIADES platform: ALCYONE and GERMINAL, in: J. Wang, X. Li, C. Allison, J. Hohorst (Eds.), Nuclear Power Plant Design and Analysis Codes - Development, Validation and Application, Woodhead Publishing Series in Energy, Elsevier, 2021, pp. 207–233. Chap. 9.
[11] S. Lemehov, F. Jutier, Y. Parthoens, B. Vos, S. Van Den Berghe, M. Verwerft, N. Nakae, MACROS benchmark calculations and analysis of fission gas release in MOX with high content of plutonium, Prog. Nucl. Energy 57 (2012) 117–124.
[12] European Commission, TRANSURANUS Handbook, Joint Research Centre, Karlsruhe, Germany, 2020.
[13] A. Magni, A. Del Nevo, L. Luzzi, D. Rozzia, M. Adorni, A. Schubert, P. Van Uffelen, The TRANSURANUS fuel performance code, in: J. Wang, X. Li, C. Allison, J. Hohorst (Eds.), Nuclear Power Plant Design and Analysis Codes -

Development, Validation and Application, Woodhead Publishing Series in Energy, Elsevier, 2021, pp. 161–205. Chap. 8.
[14] J.-F. Babelot, N. Chauvin, Joint CEA/JRC Synthesis Report of the Experiment SUPERFACT 1, Report JRC-ITU-TN-99/03, 1999.
[15] H.A. Abderrahim, P. Baeten, A. Sneyers, M. Schyns, P. Schuurmans, A. Kochetkov, G. Van Den Eynde, J.-L. Biarrotte, Partitioning and transmutation contribution of MYRRHA to an EU strategy for HLW management and main achievements of MYRRHA related FP7 and H2020 projects: MYRTE, MARISA, MAXSIMA, SEARCH, MAX, FREYA, ARCAS, Nucl. Sci. Technol. 33 (2020) 1–8.
[16] C. Prunier, F. Boussard, L. Koch, M. Coquerelle, Some specific aspects of homogeneous Am and Np based fuels transmutation through the outcomes of the SUPERFACT experiment in Phenix fast reactor, in: Global'93 Int. Conf, September 1993, pp. 12–17. Seattle, Washington, USA.
[17] C.T. Walker, G. Nicolaou, Transmutation of neptunium and americium in a fast neutron flux: EPMA results and KORIGEN predictions for the SUPERFACT fuels, J. Nucl. Mater. 218 (2) (1995) 129–138.
[18] L. Luzzi, T. Barani, A. Magni, D. Pizzocri, A. Schubert, P. Van Uffelen, M. Bertolus, V. Marelle, B. Michel, B. Boer, S. Lemehov, A. Del Nevo, Internal report describing the irradiation experiments selected for the assessment of fuel performance codes, INSPYRE Report R7.1 (2019).
[19] K. Lassmann, Uranus - a computer programme for the thermal and mechanical analysis of the fuel rods in a nuclear reactor, Nucl. Eng. Des. 45 (1978) 325–342.
[20] Y. Philipponneau, Thermal conductivity of (U, Pu)O_{2-x} mixed oxide fuel, J. Nucl. Mater. 188 (C) (1992) 194–197.
[21] H. Matzke, Gas release mechanisms in UO_2 - a critical review, Radiat. Eff. 53 (1980) 219–242.
[22] K. Lassmann, H. Benk, Numerical algorithms for intragranular fission gas release, J. Nucl. Mater. 280 (2) (2000) 127–135.
[23] P. Van Uffelen, G. Pastore, V. Di Marcello, L. Luzzi, Multiscale modelling for the fission gas behaviour in the TRANSURANUS Code, Nucl. Eng. Technol. 43 (6) (2011) 477–488.
[24] T. Barani, E. Bruschi, D. Pizzocri, G. Pastore, P. Van Uffelen, R.L. Williamson, L. Luzzi, Analysis of transient fission gas behaviour in oxide fuel using BISON and TRANSURANUS, J. Nucl. Mater. 486 (2017) 96–110.
[25] M. Charles, M. Bruet, Gap Conductance in a Fuel Rod: Modelling of the FURET and CONTACT Results, CEA, Centre d'études nucléaires de Grenoble, Grenoble, France, 1984.
[26] V. Di Marcello, V. Rondinella, A. Schubert, J. van de Laar, P. Van Uffelen, Modelling actinide redistribution in mixed oxide fuel for sodium fast reactors, Prog. Nucl. Eng. 72 (2014) 83–90.
[27] K. Lassmann, The oxired model for redistribution of oxygen in non-stoichiometric uranium-plutonium oxides, J. Nucl. Mater. 150 (1) (1987) 10–16.
[28] W. Dienst, I. Muelle-Lyda, H. Zimmermann, Swelling, densification and creep of oxide and carbide fuels under irradiation, in: Int. Conf. On Fast Breeder Reactor Performance, 5-8 March 1979, Monterey, California, USA, 1979.
[29] D. Olander, Fundamental Aspects of Nuclear Reactor Fuel Elements, Technical Information Center, Office of Public Affairs, Energy Research and Development Administration, 1976.
[30] C. Ronchi, C. Sari, Swelling analysis of highly rated MX-type LMFBR fuels; I. Restructuring and porosity behaviour, J. Nucl. Mater. 58 (1975) 140–152.
[31] T. Preusser, K. Lassmann, Current status of the transient integral fuel element performance code URANUS, in: SMiRT 7, August 1983, pp. 22–26. Chicago, USA.
[32] I. Mueller-Lyda, D. Freund, Referenzdaten zum thermischen und mechanischen Verhalten von hochdichtem Mischoxidbrennstoff, Primar Bericht 01/01/04 P43 B, Kernforschungszentrum Karlsruhe, Germany, 1980.
[33] H. Többe, Das Brennstabrechenprogramm IAMBUS zur Auslegung von Schellbrüter Brennstäben, Interatom - Technischer Bericht 75 (1975), 65.
[34] T. Barani, D. Pizzocri, F. Cappia, L. Luzzi, G. Pastore, P. Van Uffelen, Modeling high burnup structure in oxide fuels for application to fuel performance codes. Part I: high burnup structure formation, J. Nucl. Mater. 539 (2020) 152296.
[35] M. Tourasse, M. Boidron, B. Pasquet, Fission product behaviour in Phenix fuel pins at high burnup, J. Nucl. Mater. 188 (1992) 49–57.
[36] F. Cappia, B.D. Miller, J.A. Aguiar, L. He, D.J. Murray, B.J. Frickey, J.D. Stanek, J.M. Harp, Electron microscopy characterization of fast reactor MOX Joint Oxyde-Gaine (JOG), J. Nucl. Mater. 531 (2020), 151964.
[37] K. Maeda, T. Asaga, Change of fuel-to-cladding gap width with the burn-up in FBR MOX fuel irradiated to high burn-up, J. Nucl. Mater. 327 (2004) 1–10.
[38] K. Samuelsson, J.C. Dumas, B. Sundman, M. Lainet, An improved method to evaluate the 'Joint Oxyde-Gaine' formation in (U,Pu)O_2 irradiated fuels using the GERMINAL V2 code coupled to Calphad thermodynamic computations, EPJ Nucl. Sci. Technol. 6 (2020) 47.
[39] Euratom, ESNII+ - Preparing ESNII for HORIZON 2020 [Online]. Available, https://cordis.europa.eu/project/id/605172/, 2013.
[40] V. Sobolev, S. Lemehov, N. Messaoudi, P. Van Uffelen, H.A. Abderrahim, Modelling the behaviour of oxide fuels containing minor actinides with urania, thoria and zirconia matrices in an accelerator-driven system, J. Nucl. Mater. 319 (2003) 131–141.
[41] S.E. Lemehov, K. Govers, M. Verwerft, Modelling non-standard mixed oxide fuels with the mechanistic code MACROS: Neutronic and heterogeneity effects, in: IAEA-TECDOC-1416, 2003.
[42] S. Lemehov, V. Sobolev, M. Verwerft, H.A. Abderrahim, Comparative studies of different target designs for minor actinides transmutation, in: GLOBAL 2005 Int. Conf., October 2005, pp. 9–13. Tsukuba, Ibaraki, Japan.
[43] S.E. Lemehov, M. Verwerft, V. Sobolev, Thermomechanical modeling of prototypic targets containing high concentrations of minor actinides, in: Fuels and Materials for Transmutation, OECD/NEA, 2005. NEA No. 5419.
[44] M. Verwerft, S. Lemehov, M. Weber, L. Vermeeren, P. Gouat, V. Kuzminov, V. Sobolev, Y. Parthoens, B. Vos, S. Van Den Berghe, H. Segura, P. Blainpain, J. Somers, G. Toury, J. McGinley, D. Staicu, A. Schubert, P. Van Uffelen, D. Haas, OMICO oxide fuels: microstructure and composition variations final report, External Report SCK•CEN-ER- 42 (2007).
[45] S.E. Lemehov, V.P. Sobolev, M. Verwerft, Predicting thermo-mechanical behaviour of high minor actinide content composite oxide fuel in a dedicated transmutation facility, J. Nucl. Mater. 416 (1–2) (2011) 179–191.
[46] S. Lemehov, V. Sobolev, P. Van Uffelen, Modelling thermal conductivity and self-irradiation effects in mixed oxide fuels, J. Nucl. Mater. 320 (1–2) (2003) 66–76.
[47] S. Lemehov, V. Sobolev, R. Thetford, Prognosis of thermomechanical behaviour of cercer and cermet fuels in EFIT-400 transmuter, in: Int. Workshop on Technology and Components of Accelerator Driven Systems, March 2010, pp. 15–17. Karlsruhe, Germany.
[48] K. Govers, D. Terentyev, M. Hou, S. Lemehov, "Molecular dynamics study of mixed oxide fuels : issues and perspectives", in: 43rd Plenary Meeting of the European Working Group - Hot Laboratories and Remote Handling, 2005. Petten, The Netherlands.
[49] K. Govers, S. Lemehov, M. Verwerft, M. Hou, Interatomic potentials for atomic-scale simulations of UO_2, in: Enlarged Halden Programme Group Meeting - 737 Proceedings of the Fuels & Materials Sessions, vol. 2, Halden, Norway, 2007.
[50] K. Govers, S. Lemehov, M. Hou, M. Verwerft, Comparison of interatomic potentials for UO2. Part I: static calculations, J. Nucl. Mater. 366 (1–2) (2007) 161–177.
[51] K. Govers, S. Lemehov, M. Hou, M. Verwerft, Molecular dynamics simulation of helium and oxygen diffusion in $UO_{2\pm x}$, J. Nucl. Mater. 395 (1–3) (2009) 131–139.
[52] K. Govers, S. Lemehov, M. Verwerft, In-pile Xe diffusion coefficient in UO_2 determined from the modeling of intragranular bubble growth and destruction under irradiation, J. Nucl. Mater. 374 (3) (2008) 461–472.
[53] R. Delville, R&D programme for the fuel qualification of the research fast reactor MYRRHA, in: IAEA-TECDOC-CD-1689, 2011.
[54] S. Lemehov, Modeling Fuel Fragmentation and Particle Size Distribution under Normal Operation and Accidental Conditions, Mol, Belgium, 2016.
[55] S. Lemehov, MYRRHA MOX Thermo-Physical Properties: Cracked Fuel Mechanics and Axial Thermal Expansion, Mol, Belgium, 2018.
[56] V. Di Marcello, A. Schubert, J. Van De Laar, P. Van Uffelen, Extension of the TRANSURANUS plutonium redistribution model for fast reactor performance analysis, Nucl. Eng. Des. 248 (2012) 149–155.
[57] M. Bober, C. Sari, G. Schumacher, Redistribution of plutonium and uranium in mixed (U, Pu) oxide fuel materials in a thermal gradient, J. Nucl. Mater. 39 (3) (1971) 265–284.
[58] C.F. Clement, M.W. Finnis, Plutonium redistribution in mixed oxide (U, Pu)O_2 nuclear fuel elements, J. Nucl. Mater. 75 (1) (1978) 193–200.
[59] P. Konarski, J. Sercombe, C. Riglet-Martial, L. Noirot, I. Zacharie-Aubrun, K. Hanifi, M. Frégonèse, P. Chantrenne, 3D simulation of a power ramp including fuel thermochemistry and oxygen thermodiffusion, J. Nucl. Mater. 519 (2019) 104–120.
[60] P. Chakraborty, C. Guéneau, A. Chartier, Development of a complete thermo-kinetic description of cations in the mixed oxide of uranium and plutonium, in: NuFuel-MMSNF 2019 Workshop, 4-7 November 2019, PSI, Villigen, Switzerland, 2019.
[61] M. Kato, K. Maeda, T. Ozawa, M. Kashimura, Y. Kihara, Physical properties and irradiation behavior analysis of Np- and Am-Bearing MOX Fuels, J. Nucl. Sci. Technol. 48 (4) (2011) 646–653.
[62] R. Parrish, A. Aitkaliyeva, A review of microstructural features in fast reactor mixed oxide fuels, J. Nucl. Mater. 510 (2018) 644–660.
[63] D. Pizzocri, F. Cappia, L. Luzzi, G. Pastore, V.V. Rondinella, P. Van Uffelen, A semi-empirical model for the formation and depletion of the high burnup structure in UO_2, J. Nucl. Mater. 487 (2017).
[64] F. Cappia, D. Pizzocri, A. Schubert, P. Van Uffelen, G. Paperini, D. Pellottiero, R. Macian-Juan, V.V. Rondinella, Critical assessment of the pore size distribution in the rim region of high burnup UO_2 fuels, J. Nucl. Mater. 480 (2016) 138–149.
[65] J. Noirot, L. Desgranges, J. Lamontagne, Detailed characterization of high burnup structures in oxide fuels, J. Nucl. Mater. 372 (2–3) (2008) 318–339.
[66] V.V. Rondinella, T. Wiss, The high burn-up structure in nuclear fuel, Mater. Today 13 (12) (2010) 24–32.
[67] A. Gallais-During, F. Delage, S. Béjaoui, S. Lemehov, J. Somers, D. Freis, W. Maschek, S. Van Til, E. D'Agata, C. Sabathier, Outcomes of the PELGRIMM project on Am-bearing fuel in pelletized and spherepac forms, J. Nucl. Mater. 512 (2018) 214–226.
[68] M. Temmar, B. Michel, I. Ramiere, N. Favrie, Multi-physics modelling of the pellet-to-cladding gap closure phenomenon for SFR fuel performance codes, J. Nucl. Mater. 529 (2020), 151909.
[69] K. Lassmann, F. Hohlefeld, The revised URGAP model to describe the gap conductance between fuel and cladding, Nucl. Eng. Des. 103 (2) (1987) 215–221.
[70] C.F. Clement, The movement of lenticular pores in UO_2 nuclear fuel elements,

J. Nucl. Mater. 68 (1) (1977) 63–68.
[71] C. Ronchi, C. Sari, Properties of lenticular pores in UO_2, (U,Pu)O_2 and PuO_2, J. Nucl. Mater. 50 (1) (1974) 91–97.
[72] T.C. Chawla, D.L. Graff, R.C. Borg, G.L. Bordner, D.P. Weber, D. Miller, Thermophysical properties of mixed oxide fuel and stainless steel type 316 for use in transition phase analysis, Nucl. Eng. Des. 67 (1) (1981) 57–74.
[73] G. Pastore, L. Luzzi, V. Di Marcello, P. Van Uffelen, Physics-based modelling of fission gas swelling and release in UO_2 applied to integral fuel rod analysis, Nucl. Eng. Des. 256 (2013) 75–86.
[74] A. Magni, T. Barani, L. Luzzi, D. Pizzocri, A. Schubert, P. Van Uffelen, A. Del Nevo, Modelling and assessment of thermal conductivity and melting behaviour of MOX fuel for fast reactor applications, J. Nucl. Mater. 541 (2020) 152410.
[75] P. Garcia, A. Miard, Availability of Setup for Mechanical Measurements on UO_2 at CEA/DEC, INSPYRE Milestone MS8, 2019.
[76] P. Martin, G. Jouan, L. Medyk, E. Nilly, Availability of the Micro and Nano Indentation Devices at CEA/DMRC, INSPYRE Milestone MS10, 2019.
[77] D. Pizzocri, G. Pastore, T. Barani, A. Magni, L. Luzzi, P. Van Uffelen, S.A. Pitts, A. Alfonsi, J.D. Hales, A model describing intra-granular fission gas behaviour in oxide fuel for advanced engineering tools, J. Nucl. Mater. 502 (2018) 323–330.
[78] A. Cechet, S. Altieri, T. Barani, L. Cognini, S. Lorenzi, A. Magni, D. Pizzocri, L. Luzzi, A new burn-up module for application in fuel performance calculations targeting the helium production rate in (U,Pu)O_2 for fast reactors, Nucl. Eng. Technol. (2020) available online, in press.
[79] D. Pizzocri, T. Barani, L. Luzzi, SCIANTIX: a new open source multi-scale code for fission gas behaviour modelling designed for nuclear fuel performance codes, J. Nucl. Mater. 532 (2020) 152042.
[80] G. Wallez, P.E. Raison, A.L. Smith, N. Clavier, N. Dacheux, High-temperature behavior of dicesium molybdate Cs_2MoO_4: implications for fast neutron reactors, J. Solid State Chem. 215 (2014) 225–230.
[81] A.L. Smith, G. Kauric, L. van Eijck, K. Goubitz, G. Wallez, J.C. Griveau, E. Colineau, N. Clavier, R.J.M. Konings, Structural and thermodynamic study of dicesium molybdate $Cs_2Mo_2O_7$: implications for fast neutron reactors, J. Solid State Chem. 253 (2017) 89–102. May.
[82] T.R. Pavlov, F. Kremer, R. Dubourg, A. Schubert, P. Van Uffelen, Towards a More Detailed Mesoscale Fission Product Analysis in Fuel Performance Codes: a Coupling of the TRANSURANUS and MFPR-F Codes, TopFuel2018 - Reactor Fuel Performance, September 30 – October 4 2018, Prague, Czech Republic.
[83] EERA-JPNM, GEMMA European H2020 Project [Online]. Available, http://www.eera-jpnm.eu/gemma/, 2017.
[84] EERA-JPNM, EERA-JPNM website [Online]. Available, http://www.eera-jpnm.eu/, 2017.
[85] IAEA, Fuel Materials for Fast Reactors [Online]. Available, https://www.iaea.org/projects/crp/t12031, 2019.
[86] NEA, Primary Radiation Damage in Materials, vol. 9, Report NEA/NSC/DOC, 2015.